An Integrated Modelling Approach for Flight Dynamics, Manoeuvre- and Gust-Loads Analysis

Thiemo M. Kier *
German Aerospace Center (DLR), 82234 Weßling, Germany

An integrated modelling approach, suitable for flight loads analysis and flight dynamics investigations is presented. These scenarios need fast loop capable simulation models. Typically, they are evaluated many times in the entire flight envelope, for varying mass cases and for changing parameters during the aircraft design process. Further, the simulations models have very different requirements depending on their application. Flight dynamics models must account for large nonlinear rigid body motions and aerodynamic nonlinearities, manoeuvre loads analysis, additionally need to take flexible deformations into account, and hence require distributed aerodynamics, and for gust loads analysis unsteady aerodynamic effects are essential.
The proposed integrated model is based on nonlinear equations of motion using mean axes constraints. Potential flow based aerodynamics with low computational cost are the method of choice for most aeroelastic applications. Presented in this paper are some important aspects regarding the aerodynamic modelling, which are handled differently compared to other implementations.
Instead of the Doublet Lattice Method (DLM), the 3D panel method `NEWPAN` is used, which is able to capture previously neglected flight mechanical effects such as roll-yaw coupling and induced drag. Since, the Aerodynamic Influence Coefficient (AIC) matrices obtained from `NEWPAN` are nonlinearly dependent on the flight state, a Reduced Order Model (ROM) based on Proper Orthogonal Decomposition (POD) is setup and subsequently interpolated. The proposed ROM interpolates directly AIC matrices (AIC-ROM) instead of pressures. The advantages of a ROM based on AIC matrices over similar approaches based on pressure coefficients are explained. Similarly to the Doublet Lattice Method, the 3D panel code is able to compute frequency based unsteady Aerodynamic Influence Coefficient (AIC) matrices, which are approximated by a "physical" Rational Functions (RFA) to make them amenable for time domain simulations. Unlike other approaches, the physical RFA allows a clear separation of quasi-steady, added mass and unsteady lag terms.
Several application examples are presented and their particular needs are addressed. The proposed modelling approach supports flight dynamics by including previously neglected aerodynamic roll yaw coupling and nonlinear angle of attack dependencies, manoeuvre loads, including aeroelastic deformations, and gust loads analyses, including unsteady aerodynamics in one integrated model and is suitable for for investigations regarding active gust and manoeuvre load alleviation, primary flight control design, or performance improvement through lift redistribution.

I. Introduction

For many aircraft design analyses, mathematical models need to be evaluated numerous times, either to reflect changes during the design process or to evaluate certain criteria in the entire flight envelope. Therefore, loop capable models are essential, which are fast to simulate, yet accurate enough for the specific purpose. Such models for repeated evaluations are needed e.g. for loads analyses, flight control law synthesis and evaluation or for flight dynamics analyses. In these scenarios, a multitude of airspeed-altitude combinations, different mass cases and aircraft configurations, must be simulated for various manoeuvres pertaining to handling qualities and control law evaluation or for structural sizing of the aircraft. E.g., for loads analysis, the regulation specify simulation of various different design manoeuvres or flying through specific atmospheric conditions such as discrete gusts with different wave lengths or stochastic turbulence levels.

With the permutations of all the conditions mentioned above, the number of simulations can easily exceed the 100.000s. For these type of application, the use of Computational Fluid Dynamics (CFD) coupled with Computational Structural Mechanics (CSM) is still too expensive or simply inconvenient for the task at hand. Therefore, much faster aerodynamic methods are used in order to handle this large number of simulations. Usually, methods based on potential flow are employed and the missing effects are recovered by correction with higher order methods [8]. Further, linearized potential flow methods allow the formulation of so called Aerodynamic Influence Coefficient (AIC)

*Team Lead Flight Dynamics and Loads, Institute of System Dynamics and Control, AIAA Member `Thiemo.Kier@dlr.de`

matrices, which can be used to obtain the surface pressures by simple matrix multiplication with the local normal velocities at control points on the aircraft surface. This approach allows a closed formulation of equations of motion and aerodynamic forcing without the need to couple CFD and CSM codes via co-simulation.

Still, the models for flight dynamics, maneoeuvre loads and gust loads analyses have very different demands. Flight dynamics models require an accurate representation of flight mechanical effects, large nonlinear rigid body motions and the use of an aerodynamic database, describing nonlinear relationships pertaining e.g to Mach number or angle of attack. Since the manoeuvres are typically slow for transport aircraft, a quasi-steady assumption for the aerodynamics is sufficient. For manoeuvre loads analysis, flexibility of the airframe and distributed aerodynamics are necessary to reflect static aeroelastic effects. For gust loads analysis linear equations of motion are usually sufficient but need to include structural dynamics equations with distributed mass, stiffness and damping. Further, unsteady aerodynamics are required due to the fast changing onflow conditions during a gust encounter.

The integrated modeling approach proposed in [9, 10, 7, 11] has been continuously improved and yields fast, yet accurate analysis models with all appropriate characteristics required to conduct the aircraft design analyses mentioned above. The equations of motion are based on a "mean axes" formulation [6] including nonlinear rigid body motion as well as linear structural dynamics.

This paper focuses on the aerodynamic modelling requirements to suit the different kinds of analyses. For the aerodynamics model, typically Vortex [12] respectively Doublet Lattice Methods [1, 2, 3] (VLM/DLM) are employed. The DLM implementations in popular aeroelastic analysis codes like `Nastran` [13] are often lacking important features like in plane forces. However, these inplane forces are essential for the coupling of rolling and yawing motion necessary to describe flight mechanical modes like dutch roll accurately. The 3D panel code `NEWPAN` [4] models the actual surface instead of a mean plane like the DLM, and is therefore able to account for these previously missing in plane forces. `NEWPAN` can also produce AIC matrices allowing for the same direct formulation as for the classical DLM matrices, making a co-simulation approaches as described in [14] unnecessary.

The panel method AICs are obtained by linearizing about a given flight state and thus are dependent on the onflow angle. To account for this nonlinearity, a so called AIC-Reduced Order Model (AIC-ROM) approach is proposed [10, 8], where the AIC matrices as function of nonlinear parameters like angle of attack or Mach number are reduced using Proper Orthogonal Decomposition (POD) and interpolated nonlinearly.

Furthermore, the unsteady version of the 3D panel method provides complex valued AIC matrices as a function of reduced frequency for the compressible, unsteady flow regime, just like the DLM. These complex AIC matrices, containing phase information, can be used directly in frequency domain gust analyses. Time trajectories then can be obtained through inverse Fourier transformation of the spectra. For some scenarios it is more appropriate to perform aircraft analyses including unsteady aerodynamic effects directly in the time domain, e.g. when significant nonlinearites arise due an activation logic of load alleviation functions or when large nonlinear rigid bodies motions play a significant role, as during wake vortex encounters [15, 16]. Then, the tabulated frequency dependent aerodynamic matrices are fitted by a rational function approximation (RFA). For rational functions analytical Laplace transformations are available making them suitable for time domain analysis. In [9] a "physical" RFA was proposed to avoid mixed quasi-steady and unsteady aerodynamic contributions. This way unsteady aerodynamic effects can be switched on and off in a modular fashion to trade accuracy versus faster simulation speed.

The results of the 3D panel method have been validated against CFD computations. Quasi-steady liftdistributions due to roll rate and sideslip angle of the LANN wing [17] were compared and differences to the Vortex Lattice Method regarding the flight mechanic effects were highlighted. The unsteady aerodynamics were validated by applying a Fourier transformation to the time domain CFD results of a NACA64A010 airfoil subjected to sinusoidal gusts and comparison with the complex surface pressures obtained by `NEWPAN`.

Finally, the proposed integrated modelling scheme is applied to a wide range of use cases in the field of flight dynamics and loads analyses.

II. Model Integration for Flexible Aircraft Analysis

The following section describes the general principles regarding the integration aspects of the flexible aircraft analysis model, i.e. the structural model, the equations of motion and the external forcing due to propulsion and aerodynamics. These equations have been integrated in the loads environment VarLoads [18] and are expressed in closed form by the use of AIC matrices, i.e. no iterations between the structural and the aerodynamic model are necessary.

A. Structural Dynamics, Equations of Motion and Load Recovery

The starting point, when setting up the equations of motion of a flexible aircraft, is an Finite Element Model (FEM). This FEM usually consists of 100.000s of degrees of freedom (DoFs). Static condensation can be used to reduce the problem size by several orders of magnitude. The method employed is known as the Guyan reduction[19], where condensation points ($g-set$) are placed along loads reference axes. The mass distributions are prepared for the corresponding payload/fuel cases and connected to the $g-set$. Subsequently a modal analysis is carried out and only part of the modal basis is retained to further reduce the model size and computational cost.

1. Linear Aeroelastic Equations of Motion

The eigenvalues and eigenvectors define the generalized coordinates of the $h-set$. The eigenvalues with frequency zero represent the rigid body motion. Hence, the $h-set$ can be partitioned into six rigid body DoFs ($b-set$) and flexible part ($f-set$). The rigid body mode shapes $\mathbf{\Phi}_{gb}$ and the retained modes of the eigenvector matrix $\mathbf{\Phi}_{gf}$ are used to generalized the equations of motion, which are given in the frequency domain by

$$\left\{-\omega^2\begin{bmatrix}\mathbf{M}_{bb} & \mathbf{0}\\ \mathbf{0} & \mathbf{M}_{ff}\end{bmatrix} + \mathrm{j}\,\omega\begin{bmatrix}\mathbf{0} & \mathbf{0}\\ \mathbf{0} & \mathbf{B}_{ff}\end{bmatrix} + \begin{bmatrix}\mathbf{0} & \mathbf{0}\\ \mathbf{0} & \mathbf{K}_{ff}\end{bmatrix}\right\}\begin{bmatrix}\mathbf{u}_b\\ \mathbf{u}_f\end{bmatrix} = \begin{bmatrix}\mathbf{\Phi}_{gb}^{\mathrm{T}}\\ \mathbf{\Phi}_{gf}^{\mathrm{T}}\end{bmatrix}\mathbf{P}_g^{ext}(\omega). \tag{1}$$

Note that the rigid body $b-set$ DoFs in (1) are defined in a earth fixed coordinate frame.

2. Nonlinear Aeroelastic Equations of Motion

A suitable set of equations of motion to account for large rigid body motions and linear flexibility is derived in the references[5, 6]. The nonlinear equations of motion describe the movement relative to a "mean axes" body reference frame. Equations of motion for an unrestrained flexible aircraft accounting for large rigid body motions are given by

$$\begin{aligned}\begin{bmatrix}\mathbf{m}_b\left(\dot{\mathbf{V}}_b + \mathbf{\Omega}_b\times\mathbf{V}_b - \mathbf{T}_{bE}\,\mathbf{g}_E\right)\\ \mathbf{J}_b\dot{\mathbf{\Omega}}_b + \mathbf{\Omega}_b\times(\mathbf{J}_b\mathbf{\Omega}_b)\end{bmatrix} &= \mathbf{\Phi}_{gb}^{\mathrm{T}}\mathbf{P}_g^{\mathrm{ext}}(t)\\ \mathbf{M}_{ff}\ddot{\mathbf{u}}_f + \mathbf{B}_{ff}\dot{\mathbf{u}}_f + \mathbf{K}_{ff}\mathbf{u}_f &= \mathbf{\Phi}_{gf}^{\mathrm{T}}\mathbf{P}_g^{\mathrm{ext}}(t),\end{aligned} \tag{2}$$

where $\mathbf{\Phi}_{gb}$ is the rigid body modal matrix about the center of gravity and in directions as customary in flight mechanics, i.e x-forward, z-down. $\mathbf{V}_b$ and $\mathbf{\Omega}_b$ are the velocity, respectively angular velocity vectors in the body frame of reference. The matrix $\mathbf{T}_{bE}$ transforms the gravitational vector from an earth fixed (E) to the body fixed coordinate frame (b) as a function of Euler angles.

3. Load Recovery by Force Summation

In order to recover the nodal loads $\mathbf{P}_g$ for a subsequent sizing of the structure, the force summation method (FSM) [20] is employed. Thus, subtraction of the inertial loads $\mathbf{P}_g^{\mathrm{iner}}$ from the external loads, yields

$$\mathbf{P}_g = \mathbf{P}_g^{\mathrm{ext}} - \underbrace{\mathbf{M}_{gg}\left\{\mathbf{\Phi}_{gb}\,\ddot{\mathbf{u}}_b \quad + \quad \mathbf{\Phi}_{gf}\,\ddot{\mathbf{u}}_f\right\}}_{\mathbf{P}_g^{\mathrm{iner}}} \tag{3}$$

In the case of the nonlinear equations of motion (2), the rigid body acceleration is given as

$$\ddot{\mathbf{u}}_b = \begin{bmatrix}\dot{\mathbf{V}}_b + \mathbf{\Omega}\times\mathbf{V}_b - \mathbf{T}_{bE}\,\mathbf{g}_E\\ \dot{\mathbf{\Omega}}_b + \mathbf{J}_b^{-1}\left(\mathbf{\Omega}_b\times(\mathbf{J}_b\mathbf{\Omega}_b)\right)\end{bmatrix}. \tag{4}$$

The FSM requires the external forces to be available on the structural grid. This allows to account for the static part directly on the physical grid. Therefore, the dependence on the number of retained flexible modes is abated which improves the convergence behavior significantly.

Internal loads at cut stations can be computed by integrating the nodal loads along the loads reference axes of each aircraft component. A loads envelope is generated by taking the maximums and minimums of each individual quantity. Correlated loads, where e.g. torsion and bending moments are correlated in time, form a trajectory in a 2D plane. The extremes of this convex hull, some times referred to as potato plots are also important quantities of interest. The resulting quantities in the loads envelope are used as sorting criteria to obtain the critical load cases used for the structural sizing of the structural components.

B. Potential Flow Aerodynamic Models: 3D Panel and Doublet Lattice Method

The major contribution to the external forces apart from the propulsion forces stem from the aerodynamics. So called Aerodynamic Influence Coefficient matrices based on linear potential flow theory have classically been used for aeroelastic applications.

1. Governing Flow Equations

The governing flow equations for the panel method as well as the DLM are the unsteady linearized potential flow equations, sometimes also referred to as the unsteady Prandtl-Glauert equations. The derivation of methods based on potential flow starts out with the steady velocity potential Φ_S.

$$\left(1 - M_\infty^2\right) \frac{\partial^2 \Phi_S}{\partial x^2} + \frac{\partial^2 \Phi_S}{\partial y^2} + \frac{\partial^2 \Phi_S}{\partial z^2} = 0 \tag{5}$$

Using a Göthert Type 2 transformation [21], the problem can be reduced to a Laplace type equation $\nabla^2 \Phi_S = 0$.

The Vortex Lattice Method (VLM) solves the velocity potential equation by discretizing the mean lifting surface by so called horseshoe vortices, where the bound vortex lies on the quarter chord of each box and the trailing vortices extend to infinity. The forces are then calculated by application of the Kutta Jokowsky Law, where the circulation is related to lift. In the case of the steady panel method the actual and not the mean surface is discretized. The basic solutions chosen are velocity potential source and doublet panels. The result is a velocity potential distribution. Differentiation of the this velocity potential in the spatial directions yield the flow velocities on the surface, which in turn can be used to determine the surface pressures and ultimately the lifting forces.

This steady solution about a, possibly deformed, reference shape defines the flight state about which an unsteady linearization is performed. The unsteady solution is then found by solving the linearized frequency domain variant of the unsteady Prandtl-Glauert equation

$$\left(1 - M_\infty^2\right) \frac{\partial^2 \Phi_U}{\partial x^2} + \frac{\partial^2 \Phi_U}{\partial y^2} + \frac{\partial^2 \Phi_U}{\partial z^2} - 2\mathrm{j}\omega \frac{M_\infty}{a_\infty} \frac{\partial \Phi_U}{\partial x} - \left(\frac{\omega^2}{a_\infty^2}\right) \Phi_U = 0, \tag{6}$$

where the unsteady potential is given as $\mathrm{e}^{\mathrm{j}\omega t}\ \Phi_U(x, y, z)$. Application of a Galilean transform converts eq. (6) to a Helmholtz type partial differential equation

$$\nabla^2 \Phi_U + \kappa^2 \Phi_U = 0, \quad \text{with} \quad \kappa = k \frac{M_\infty}{1 - M_\infty^2} \tag{7}$$

to determine the solution, where κ is a frequency parameter depending on the reduced frequency $k = \frac{c_{\mathrm{ref}}/2}{U_\infty}\omega$ and Mach number.

The total velocity potential is then $\Phi(x, y, z, \omega) = \Phi_S(x, y, z) + \mathrm{e}^{\mathrm{j}\omega t}\ \Phi_U(x, y, z)$, In the case of the unsteady panel method, this expression is used to calculate the complex unsteady pressure via a linearized version of the unsteady Bernoulli equation. The Doublet Lattice Method (DLM) also provides a harmonic solution for equation (6), with some notable differences. The DLM uses the acceleration potential which is formally equivalent to the velocity potential equation. Therefore, the same elementary solutions are valid, e.g. the doublet potential. The acceleration potential readily yields the pressure difference between the upper and lower surface. Since there is no pressure jump across the wake, it can be omitted in the modeling process. Further, due to the linearization applied in the derivation of the DLM, the coupling between the steady and unsteady flow is lost, which is accounted for by the 3D panel method intrinsically.

2. Aerodynamic Influence Coefficient Matrices and Boundary Conditions

Both described aerodynamic methods have in common the concept of the frequency dependent Aerodynamic Influence Coefficient (AIC) matrix. The AIC matrix relates a normal wash at a control point to a pressure at each of the discretization elements for discrete harmonic excitations in the frequency domain. When calulated over a range of reduced frequencies k, transfer functions relating normal wash excitations to pressures can be determined.

The pertubation pressures $\Delta\, \mathbf{c_p}$ about the steady state can be calculated with the following equation:

$$\Delta\, \mathbf{c_p}_j(k) = \left[\mathbf{Q}_{jj}\ \left(\mathbf{D^x}_{jk} + \mathrm{j}k \cdot\ \mathbf{D^t}_{jk}\right)\ + \left(\mathbf{DP^x}_{jk} + \mathrm{j}k \cdot\ \mathbf{DP^t}_{jk}\right)\right]\ \mathbf{u}_k(k), \tag{8}$$

where the matrix $\mathbf{D^x}_{jk}$ accounts for a change in downwash due to a change of the normal vector with respect to the free stream direction and the matrix $\mathbf{D^t}_{jk}$ for additional downwash due to movement of the boundary in direction of the

panel normal. When thick bodies are modeled in potential flow, additional pressure contributions arise. These are not associated with the normalwash, but with tangential flow at the panels. Therefore, the 3D Panel Method, requires the additional motion induced terms $\mathbf{DP^x}_{jk}$ and $\mathbf{DP^t}_{jk}$. It should be noted that these terms are dependent on the onflow direction, i.e. they are associated with the flight state, about which the AIC was linearized. For thin velocity potential panels as well as in the DLM these terms are zero. The vector $\mathbf{u}_k(k)$ describes the motion of the individual panels at their reference point, which may result from rigid body motion, flexible deformation or control surface deflections.

If the excitation is not motion induced, but a result from atmospheric disturbances, the downwash due to these have to be determined in the frequency domain. E.g. the spectrum for a discrete tuned $\mathbf{v}_G(\omega)$ is available in a frequency dependent semi-analytically form with parameters like the gust gradient length. Further, when the aircraft is subjected to the gust, the penetration speed U_∞ and location of the control points $\mathbf{x}_j$ wrt. the gust need to be considered. In the frequency domain these time lags are expressed as phase shifts with an exponential function.

$$\mathbf{w}_j^G(\omega) = \mathbf{n}_j \cdot \exp\left(-\mathrm{j}\omega \cdot \mathbf{x}_j / U_\infty\right) \cdot \mathbf{v}_G(\omega)/U_\infty \tag{9}$$

The dot product with $\mathbf{n}_j$ then determines the direction for vertical, lateral or head-on gusts.

3. Pressure Integration and Grid Interpolation

The load transformation to panel reference point is done by integrating the pressures, which is mostly a simple multiplication with the aerodynamic box area. Depending on the method, an offset between force application location and the panel reference point may be present. The respective moment arms are accounted for by the integration matrix $\mathbf{S}_{kj}$, if rotational degrees of freedom are introduced in the aerodynamic $(k-set)$. Multiplication with the dynamic pressure yields the aerodynamic forces.

$$\mathbf{P}_k^{\text{aero}} = q_\infty \, \mathbf{S}_{kj} \, \mathbf{c_p}_j \tag{10}$$

Finally, the aerodynamic loads have to be mapped to the structural degrees of freedom. The matrix connecting the displacements of the structural grid $(g-set)$ to the aerodynamic grid $(k-set)$ is called spline matrix $\mathbf{T}_{kg}$.

$$\mathbf{u}_k = \mathbf{T}_{kg}\mathbf{u}_g \tag{11}$$

This mapping is achieved, e.g. by employing radial basis functions, such as the commonly used Infinite Plate Spline (IPS), or by using beam splines [22, 23]. The physical interpretation is that the structure behaves plate or beam like and that the respective degrees of freedom sets $k-set$ and $g-set$ lie on the same structural entity described by the spline basis functions. The aerodynamic loads can be mapped back onto the structure with the transpose of the spline matrix, based on the principle of virtual work.

$$\mathbf{P}_g^{\text{aero}} = \mathbf{T}_{kg}^{\mathrm{T}}\mathbf{P}_k^{\text{aero}} \tag{12}$$

Pre-multiplication with the transpose the modal matrix $\mathbf{\Phi_{gh}}$ yield the generalized aerodynamic forces, compatible with the equations of motion (1) and (2). The entire product,

$$\mathbf{Q}_{hh}(k) = \mathbf{\Phi}_{gh}^{\mathrm{T}} \, \mathbf{T}_{kg}^{\mathrm{T}} \, \mathbf{S}_{kj} \left[\mathbf{Q}_{jj}(k) \, \left(\mathbf{D^x}_{jk} + \mathrm{j}k \cdot \, \mathbf{D^t}_{jk}\right) \, + \left(\mathbf{DP^x}_{jk} + \mathrm{j}k \cdot \, \mathbf{DP^t}_{jk}\right)\right] \, \mathbf{T}_{kg} \, \mathbf{\Phi}_{gh} \tag{13}$$

is often referred to as Generalized Aerodynamic Force (GAF) matrix.

III. Steady and Unsteady Aerodynamics

To facilitate sufficiently fast aerodynamic computations for the targeted applications necessitates some simplifications in the derivation of the governing flow equations.

The starting point are the Navier-Stokes equations, which consist of three conservation laws, namely the conservation of momentum in the three spatial dimensions, the conservation of mass and the conservation of energy, to determine the value of five state variables. The cancellation of viscosity related terms lead to Euler's equation. Due to its inviscid nature, no boundary layer and hence no viscous drag is present anymore. When further the flow is assumed to be irrotational, a scalar potential can be introduced and the full potential equations emerge. According to Crocco's theoreme an irrotational flow is also isentropic, i.e no strong shocks can be captured anymore. The formulation still allows for supersonic pockets, however the terminating shock must be weak, since strong shocks are associated with a jump in entropy. If further small disturbances in the y- and z-direction are assumed, the equation simplifies to the so called Transonic Small Disturbance equation (TSD), which is still capable to capture transonic effects, however blunt bodies can not be evaluated. Linearization, finally leads to the aforementioned unsteady Prandtl-Glauert equation (6).

The solution is only valid for either purely subsonic or purely supersonic flow regimes. No transonic effects can be captured and have to be accounted for by correction terms, e.g. as proposed in [8] if deemed necessary.

The 3D panel method NEWPAN [4] solves eq. (6) just like the Doublet Lattice Method by applying a Boundary Element Method (BEM), i.e. the flow field can be computed without the necessity to discretize the volume around the aircraft like in classical CFD methods, but merely its surface. Both methods provide AIC matrices, which allow a direct and closed formulation of the equations of motion, i.e. no iterative scheme to pass deformations and aerodynamic forces between two applications is necessary. These AIC matrices are obtained as a function of reduced frequency. To make them amenable for time domain simulations, a suitable procedure known as Rational Function Approximation (RFA) is applied.

The panel method NEWPAN can account for thickness effects and computes surface pressures, whereas the DLM represents mean lifting surfaces and computes only pressure differences between the upper and lower side. Further the panel code considers a non linear dependence on flow direction, which is lost for the DLM due to the way the underlying formulation was obtained. A direct consequence is the presence of inplane forces, which are the basis for important flight mechanical coupling effects. These were previously unavailable in classical Vortex/Doublet Lattice implementations, e.g. as used in the popular aerolastics code NASTRAN.

A. Validation

To validate the results and demonstrate the capability to capture the flight mechanical and unsteady gust effects, a comparison of the 3D panel method with a CFD code solving Euler type governing equations is presented. Highlighted are also the differences to DLM results, in particular with regard to the flight dynamics aspects.

1. Steady Angle of Sideslip and Roll Rate

The chosen test case is the LANN wing [17]. The half wing is mirrored to obtain results for the lateral unsymmetric flow conditions. It has no dihedral and a cambered airfoil. To stay within the validity range of the governing equations of the potential flow the flight state was set at a subsonic Mach number of $Ma = 0.65$ and an angle of attack $\alpha = 0°$. Then spanwise lift distribution gradients due to sideslip angle β and roll rate p are computed by simple finite differences for the CFD calculations. Distributions for the 3D panel are obtained by multiplication of the steady ($k = 0$) AIC matrix with the corresponding boundary condition matrices, c.f. eq. (8).

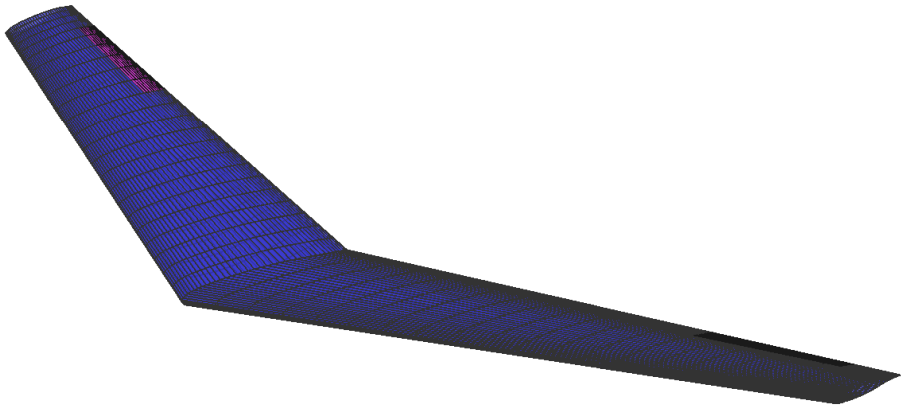

Figure 1. Panel mesh of LANN wing.

The first effect to be examined is the rolling moment due to sideslip C_{L_β}. The perturbation step was $1°$ for the sideslip angle β. The panel method results show excellent correlation with the CFD results for all of the gradient distributions in drag and lift, depicted in figure 2. As expected, the "classical" VLM is not able to capture any of these effects associated with sideslip. Integration of the lift over span, yields the desired rolling moment coefficient C_{L_β}.

Another effect is the yawing moment due to roll rate C_{N_p}. Lift and Drag distributions are shown in figure 3. The lift distribution is well captured by both potential flow methods. The forces in x-direction are induced by a change of angle of attack along the wing span due to the roll rate. Since the "classical" VLM does not capture the change in direction of lift, those forces are zero. In contrast, the panel method shows an distribution of the forces in x, however, somewhat lower when compared to the CFD results. The value for the yawing moment coefficient C_{N_p} is obtained by integration of the distribution over the span.

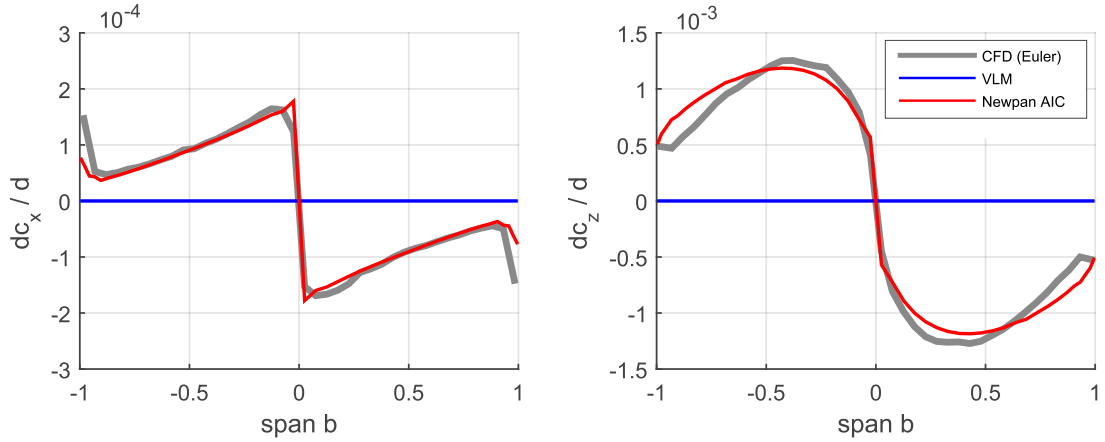

Figure 2. Drag, lift, and moment gradient distribution due β.

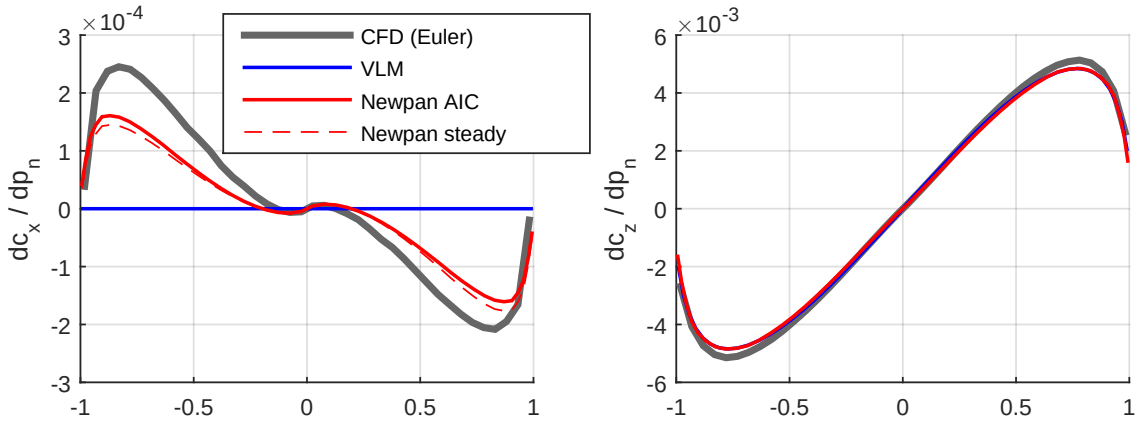

Figure 3. Drag and lift gradient distribution due roll rate p_n.

2. *Unsteady Gust excitation*

To validate the gust induced pressures, a 2D airfoil test case was selected. For the CFD calculations a NACA64A010 airfoil was subjected to a sinusoidal gust excitation. Again, subsonic conditions were chosen ($Ma = 0.6$) and the gust frequency k_G was varied to simulate several gust lengths. In the time domain a sufficient number of cycles was computed to ensure that any transients are decayed. A Fourier transform is applied to the surface pressures which are then compared to the 3D panel results. The model for the 3D panel method consisted of a high aspect ratio half wing with approximately the same chordwise discretization as the CFD mesh. To minimize 3D effects, the center section of the resulting complex pressures are compared to the CFD results. Figure 4) shows the complex gust velocities and

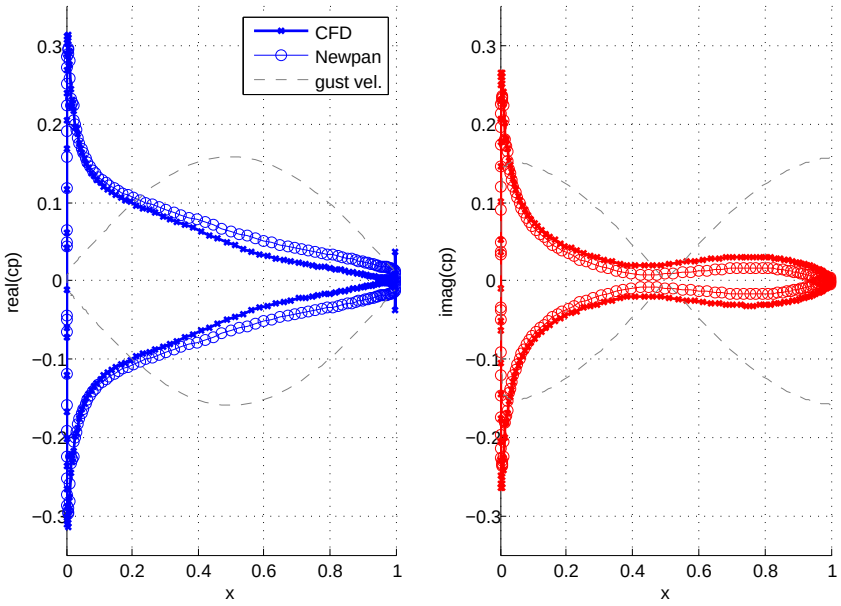

Figure 4. Complex pressure distribution of a symmetric airfoil due to a sinusoidal gust with $k_G = 1.5$.

pressure coefficients from the panel method as well as the Euler type CFD calculation. The left hand side depicts the real and the right hand side the imaginary parts. Results for the case of $k_G = 1.5$ compare excellently, for the complex pressure coefficients. The unsteady panel method `NEWPAN` is capable to accurately describe the pressures related to gust excitations.

B. Rational Function Approximation

The AIC matrices are tabulated for discrete reduced frequencies. A Rational Function Approximation (RFA), where the frequency domain transfer functions are fit with suitable "rational" terms can be used to make them amenable for time domain integration. For rational functions, a Laplace transformation exists and therefore the unsteady aerodynamics can be cast in state space form. Many flavors of this method have been published in literature [24, 25, 26, 27]. Fitting of the AICs $\mathbf{Q}_{jj}(k)$ without multiplication with differentiation matrices in eq. (8) has been proposed in [9]:

$$\mathbf{Q}_{jj}(\hat{s}) = \mathbf{Q^0}_{jj} + \mathbf{Q^1}_{jj}\hat{s} + \sum_{i=1}^{n_p} \mathbf{Q^{L}}_{i\,jj} \frac{\hat{s}\mathbf{I}}{\hat{s} + p_i}, \tag{14}$$

where $\hat{s} = s\left(\frac{c_{ref}/2}{U_\infty}\right)$ is the Laplace domain equivalent to the reduced frequency k.

This "physical" RFA (14) has several advantages over the approximation of the generalized aerodynamic forces. E.g., the fit is not tied to a particular mass case and it allows to apply the time delays directly without approximation of the gust column. Take note of the missing second derivative in the approximation. If the differentiation matrices of eq. (8) and hence the additional time derivative are applied before the RFA, mixed quasi-steady and unsteady contributions arise. Further details can be found in reference [9].

Another advantage of the "physical" RFA is the clear distinction between the quasi-steady and unsteady effects respectively the associated physical interpretation of each of the terms. $\mathbf{Q^0}_{jj}$ accounts for the quasi-steady aerodynamics, $\mathbf{Q^1}_{jj}$ is the non-circulatory added mass term and $\mathbf{Q^{L_i}}_{jj}$ represents the time lag terms, typically due to wake convection.

It should be noted that, strictly speaking the added mass term is only present in the incompressible flow regime. For compressible flow, pressure waves are propagated with the speed of sound and the added mass term vanishes. Hence, two different time delay mechanisms arise, one from the convection of the wake vorticity and one from pressure wave propagation in upstream and downstream direction. Since these might have different time scales, the number of poles should be increased when compressible flow is considered.

In the context of a spectral gust loads analysis, the RFA also allows a convenient evaluation in the frequency domain and constitutes another scheme for interpolation.

C. Nonlinear Interpolation: steady AIC-ROM

The AIC matrices of the 3D panel method depend nonlinearly on the flight state, unlike the VLM, where there is no such dependency. Therefore, the AICs have to be computed for range of parameters in the flight envelope and an appropriate scheme to interpolate between them is required.

The proper orthogonal decomposition (POD), also known as principle components analysis or Karhunen Loéve expansion, is a commonly used order reduction method with a broad range of applications, fluid dynamic problems being among them [28]. In general, it is a linear method which establishes an optimal basis, or modal decomposition, of an ensemble of continuous or discrete functions. The goals of applying the POD here are twofold: the POD enables to exploit similarity within a cluster of panel method results in a subspace of the flight envelope, thereby preserving the essential information by means of a only a few basis vectors. More importantly, paired with interpolation, any desired flight condition within this subspace can be approximated, producing a reduced order model (ROM). This ROM can then be evaluated efficiently in transient manoeuvre loads simulations.

The novelty of the approach described in [7] and [8] is that the POD is applied to AIC matrices rather than pressures, i.e. it is not necessary to build up a ROM for all parameters required in the simulation, but only for those parameters where the major nonlinearities occur, e.g. α and β. All other parameters like flexibility, rotation rates, or control surface deflections can be deduced from the AIC matrix gradient information in a linearized fashion about the nonlinearly interpolated flight state.

This AIC-ROM consists of two distinct PODs, one for the AIC matrices, i.e. the gradient information, and one for the pressure intercepts. The latter is similar to the classical pressure ROMs, as one value per panel is treated. For the first POD, the individual AIC matrices are reshaped as column vectors of length n^2_{panels}, to setup the snapshot matrix. Considerations of energy preservation then lead to the number of retained eigenvectors used for the AIC-ROM and hence to the amount of data compression. The interpolation for the nonlinear flight state variables is based on the thin plate spline (TPS); but other schemes are of course also possible. More details on the proposed approach can be found in [8].

Once more, the LANN wing was chosen to compare the results AIC-ROM with direct `Newpan` computations. First, a set of flight states was chosen to set up the AIC-ROM with a fixed Mach number of $Ma = 0.65$. `USNewpan` was then used to compute the quasi-steady AIC matrices for $k = 0$ about four different flight states, i.e. for a range of angles of attack $\alpha = 0°, 5°, 10°$ with $\beta = 0°$ and a side slip case at $\alpha = 0°$ with $\beta = 10°$. The POD for the AIC matrices was setup and all eigenvectors were retained.

The AIC-ROM is evaluated at a random flight state using the previously described procedure and compared to the results of a steady panel method run, cf. figure 5. The flight state selected for this case is $\alpha = 8°$, $\beta = 1°$, $p_n = 1.5°/s$, $\delta_{\text{ail}} = 10°$. Further the flight state was also computed using a single AIC matrix linearized about $\alpha = 0°$, $\beta = 0°$. The agreement of the AIC-ROM evaluation and the steady reference calculation is excellent. Also the necessity to use interpolated AICs becomes evident when comparing the results to the distributions evaluated with a single AIC far away from the linearization point.

In this example, the advantages of the AIC-ROM become apparent. The ROM was setup only with AIC matrices related to the (nonlinear) flight parameters α and β. The other parameters roll rate p_n and aileron deflection δ_{ail} are inferred from the linear gradient information of the AIC matrices. This is particularly useful for aeroelastic simulations, where the structural flexibility can be treated in the same way. If the ROM was set up using directly the pressures instead of the AICs, the parameter space for aeroelastic simulations would be vastly increased.

Further, the evaluation of the AIC-ROM during the simulation can be sped up significantly by generalizing the retained pressure eigenvectors of the POD. In a postprocessing step the pressures can be retrieved by reevaluating the AIC-ROM with the full eigenvectors, e.g. for visualization or load recovery.

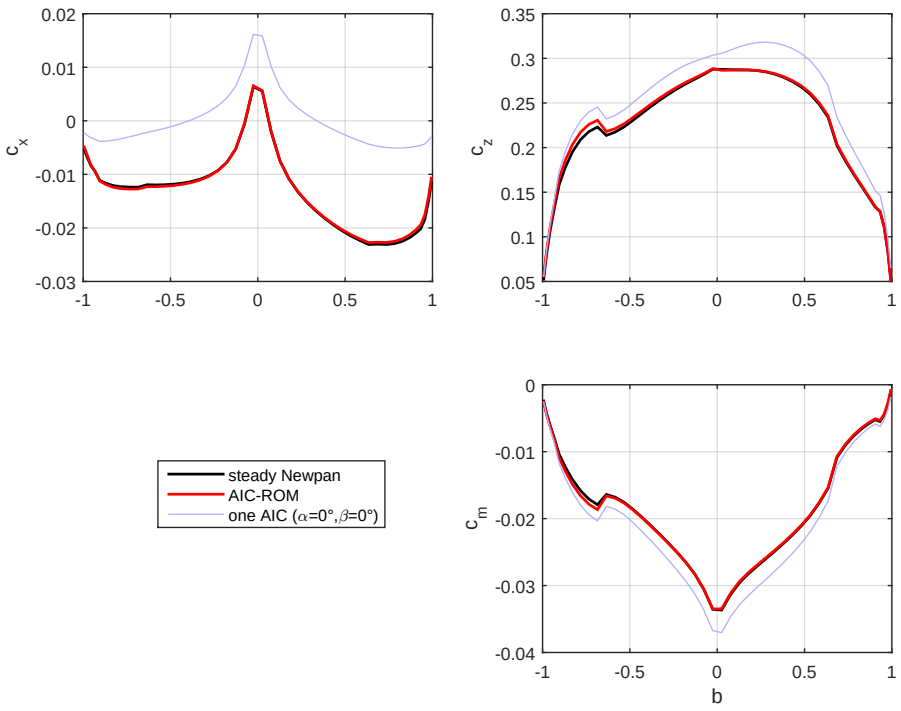

Figure 5. Drag, lift, and moment distributions at flight state $\alpha = 8°$, $\beta = 1°$, $p_n = 1.5°/s$, $\delta_{\text{ail}} = 10°$. Comparison of a reference calculation, the AIC-ROM, and using a single AIC matrix at linearization point $\alpha = 0°$, $\beta = 0°$

IV. Applications

The described modelling scheme has been applied to various uses cases, ranging from flight dynamics analysis to the determination of flight loads. Depending on the particular needs of each use case, e.g. the inclusion of unsteady aerodynamics in gust loads, the corresponding components were added. The following section will describe a few of the application scenarios and highlight the required features of the model integration.

A. Flight Mechanical Modes

The Doublet Lattice Method does not support inplane aerodynamic forces in its standard implementations. This has an influence on the classical flight mechanical modes, in particular on the dutch roll mode, where the roll-yaw coupling plays a major role. During a lateral gust encounter, the dutch roll might be excited and significantly influence the loads on the vertical tailplane. The 3D panel method supports inplane forces. Hence, the two aerodynamic methods and their differences with respect the frequency and damping of the flight mechanical modes can be assessed.

In [11] a T-tail transport aircraft configuration was used to compare the panel method 6a and the DLM 6b.

Since the target application was a lateral gust loads analysis, the integrated models included flexible structural dynamics, as well as unsteady aerodynamics realized by a Rational Function Approximation. When the model is linearized about its trimmed state, a eigenvalue analysis results in a typical pole plot depicted in figure 7. The eigenvalues can be categorized in flexible modes, aerodynamic lag states and flight mechanical modes.

	Dutch Roll Mode	
	f	g
DLM	0.26692 Hz	0.21643
3D Panel Method	0.26457 Hz	0.16639

Table 1. Dutch roll frequencies and damping for reference and increased dihedral configuration.

The frequencies and damping ratios of the dutch roll modes for each of the aerodynamic methods are summarized in table 1.

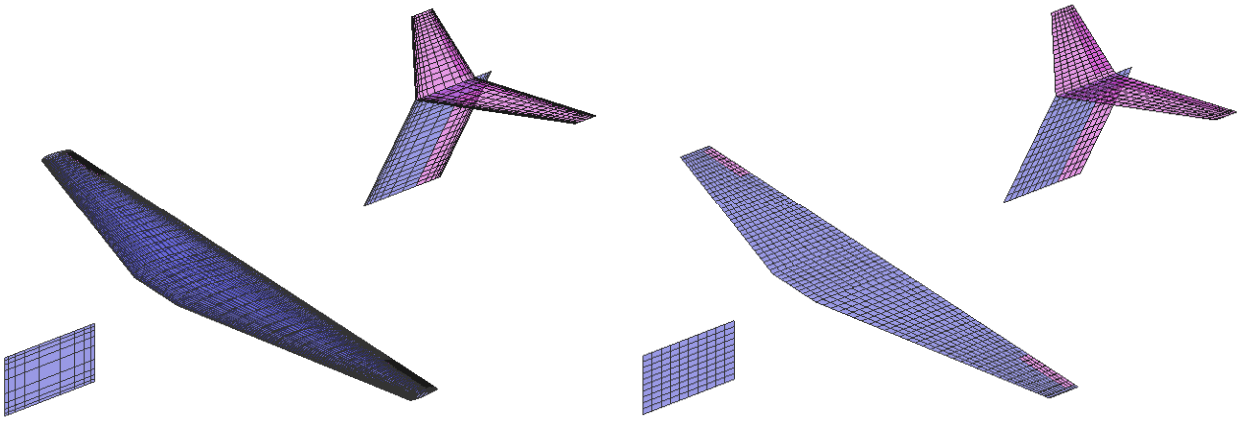

a) Panel method grid

b) DLM grid

Figure 6. High wing T-tail configuration: aerodynamic grids

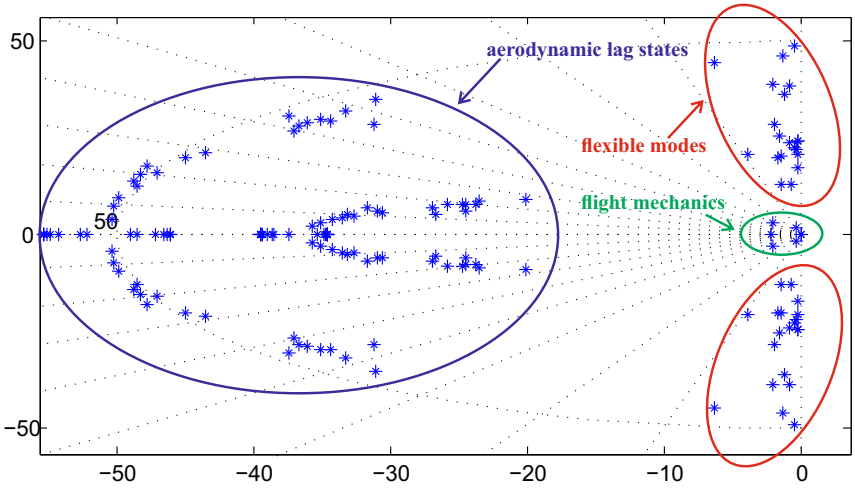

Figure 7. pole plot for fexible aircraft with unsteady aerodynamics

The frequencies of the dutch roll mode for the DLM and the panel method are almost identical. However, there is a significantly reduced damping in the case of the 3D panel code. This can be attributed to the missing flight mechanical effects in the DLM.

B. Manoeuvering Flexible Aircraft

The missing inplane forces also have a significant impact on the manoeuvering aircraft. The most prominent effect is the so called "adverse yaw", where the inplane components of the aerodynamic forces lead to a yawing moment opposite to the aircraft rolling direction.

When very flexible aircraft are considered, also the modal deflections can produce significant inplane aerodyanmic forces. Figure 8 depicts the forces in x- and z-direction, as well as the moment about the y-axis for a roll excitation and due to deflection of the second flexible mode (antisymmetric wing bending). While the forces and torsion moments

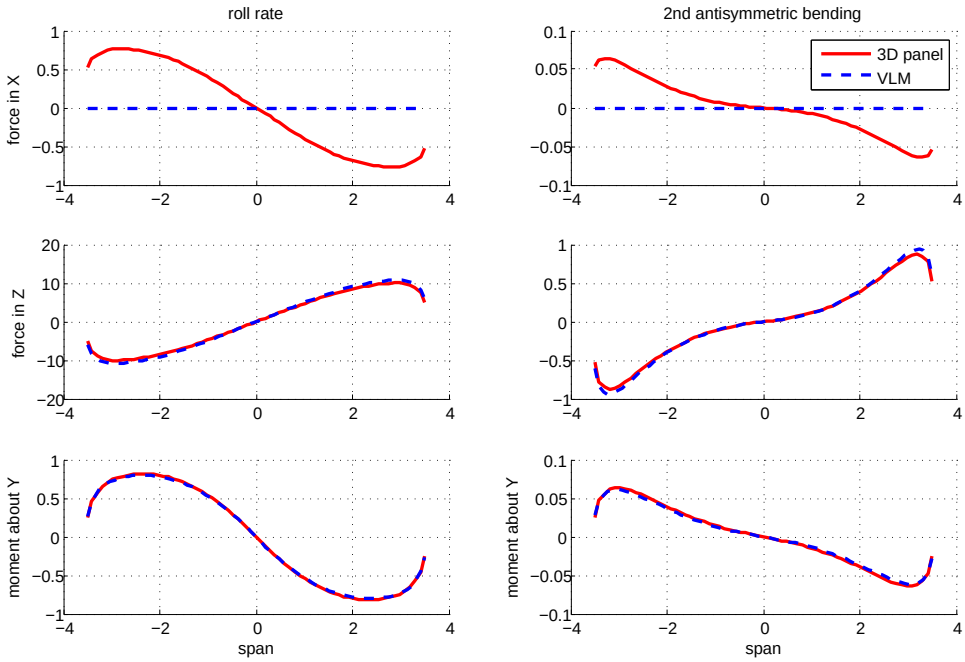

Figure 8. Drag, lift, and moment distributions due to a roll rate p_n and modal deflection of the second wing bending mode

are accurately captured, the classical VLM/DLM implementations fail to produce the inplane forces and therefore neglect the resulting adverse yawing moments. However, not only the rigid body aerodynamics, but also the flexible deformation might have a significant contribution to the yawing moment. Hence, an aerodynamic method should be chosen, which is able to take these forces into account, when flight dynamics simulations of very flexible aircraft are considered.

C. Static and Dynamic Manoeuvre Loads

One of the most prominent use cases for flexible aircraft model is the loads analysis for the structural sizing of the airframe. The load conditions to be considered for large airplanes are specified in the CS25 subpart C [29]. The determination of flight loads can be separated into gust loads and manoeuvre loads analysis, which typically use different kind of models. For gust loads unsteady aerodynamic effects are of major importance, while for manoeuvre loads usually a quasi-steady aerodynamic approximation suffices. The paragraphs for some of the load conditions are listed here:

- CS 25.331 Symmetrical Maneuver
- CS 25.349 Rolling Conditions
- CS 25.351 Yaw Maneuver Conditions
- CS 25.367 Antisymmetrical Loads due to Engine Failure

Some of these load conditions are solved by trimming the aircraft, e.g. the 2.5 g pull up for the symmetrical manoeuvre condition. Figure 9 depicts a transport category aircraft with considerable wing flex due the load factor $N_z = 2.5$. Due to the high load factor, the large deformation occurs which considerably alters the lift distribution compared to the rigid aircraft.

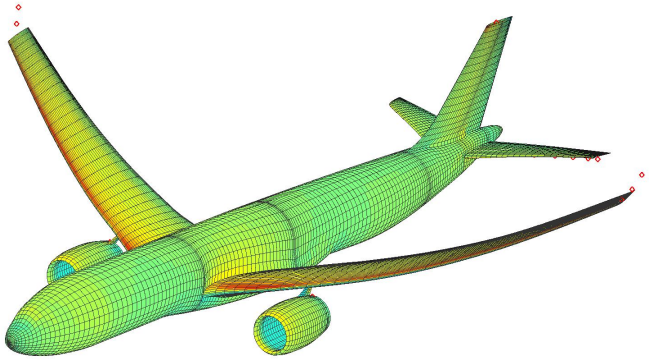

Figure 9. pressure distribution due to a 2.5 g pull-up manoeuvre using an AIC based 3D panel method approach.

Other load conditions might require time simulations, in particular when the aircraft dynamics are augmented by an active flight control system. The yaw manoeure condition, important for sizing of the VTP structure is specified in CS 25.352. Aircraft are usually equipped with a yaw damper control law to reduce the adverse effect of the aforementioned dutch roll mode and a rudder travel limitation, which schedules the maximum allowed control surface deflection with dynamic pressure. The manoeuvre starts from a trimmed horizontal flight. Then, the pilot commands a

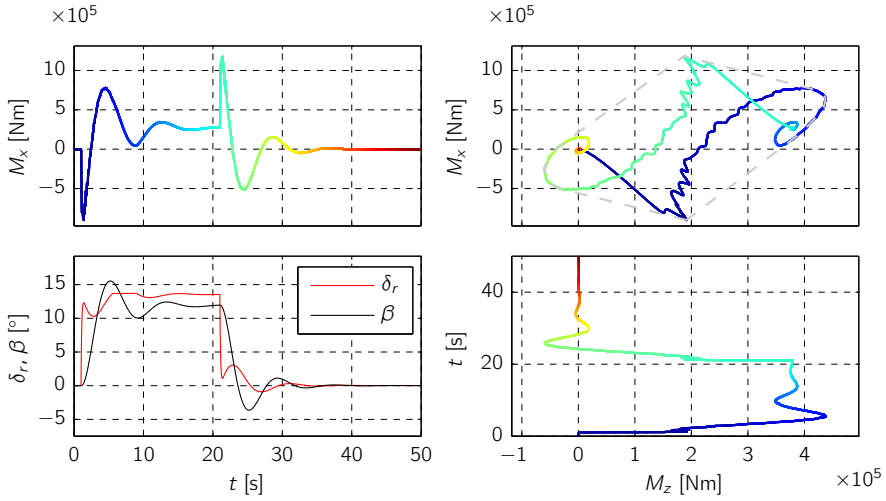

Figure 10. Correlated VTP root bending and torsion Loads during yaw manoeuvre

step input to the pedals and the rudder is deflected, exerting a side force on the tailplane. The sidedeslip angle β builds up and might dynamically overshoot its steady value. The β_{max} correlates with the maximum torsional loads. Once a steady sideslip angle is established, the pedal command is suddenly returned to zero. The missing counterforce of the rudder control surface, results in a side force in the opposite direction which yields the maximum bending loads. The resulting bending and torsion moments at the VTP root over time are found in figure 10. Correlating the bending and torsion moments, results in a so called potato plot used to size the empennage structure accordingly.

The graph of the rudder deflection due to the step command of the pilot clearly shows the effect of the yaw damper control function. Trade offs between flight mechanical reponse, ride comfort and loads need to be considered when designing control functions. Simulation results for a parametric gain variation of the yaw damper control law can be found in [30].

D. Discrete Gust Loads

In CS 25.341 of the regulations, requirements for discrete 1-cos shaped gusts are specified. The use case is the same T-tail transport aircraft [11] of figure 6 used previously for the comparison of dutch roll modes. The frequency dependent, complex AIC matrices of `USNEWPAN` with the discretization depicted in figure 6a were used for a frequency domain gust analysis.

The frequency domain gust equation is derived from the linear equations of motion (1), by solving for the generalized deformations $\mathbf{u}_h$. The gust equation then reads:

$$\left[-\omega^2\mathbf{M}_{hh} + \mathrm{j}\,\omega\mathbf{B}_{hh} + \mathbf{K}_{hh} - q_\infty\mathbf{Q}_{hh}(\omega)\right]\mathbf{u}_h(\omega) = q_\infty\mathbf{Q}_{hG}(\omega), \tag{15}$$

where $\mathbf{Q}_{hG}$ is the generalized AIC matrix for the gust input. To derive this matrix, the AIC matrix is multiplied with the vector of time delays to the individual panels, i.e. eq. (9) but without the specific gust spectrum $\mathbf{v}_G(\omega)$. Once solved for the transfer functions, results for different gust spectra can be calculated by simple matrix multiplications within seconds. Once the generalized deformations $\mathbf{u}_h(\omega)$ are computed, the loads are recovered with the force summation method:

$$\mathbf{P}_g(\omega) = \underbrace{q_\infty\left[\mathbf{Q}_{gG}(\omega) + \mathbf{Q}_{gh}(\omega)\mathbf{u}_h(\omega)\right]}_{\mathbf{P}_g^{\mathrm{ext}}} - \underbrace{\left[-\omega^2\mathbf{M}_{gh}\mathbf{u}_h(\omega)\right]}_{\mathbf{P}_g^{\mathrm{iner}}}. \tag{16}$$

Integration of the individual loads P_g along the structural component, leads to the internal cut loads, which the structure has to be sized against. Please note, that the subscript capital G refers to the gust, whereas g is the physical, structural degree of freedom set.

The AICs obtained from `USNEWPAN` for eight reduced frequencies up to $k = 4.0$ were used to set up a rational function approximation as described in section B. The RFA can be used as an interpolation scheme in the frequency domain by replacing the Laplace variable of equation (14) with the reduced frequency. Interpolation of 512 frequencies up to $k_{max} = 1.2$ yields nicely resolved transfer functions.

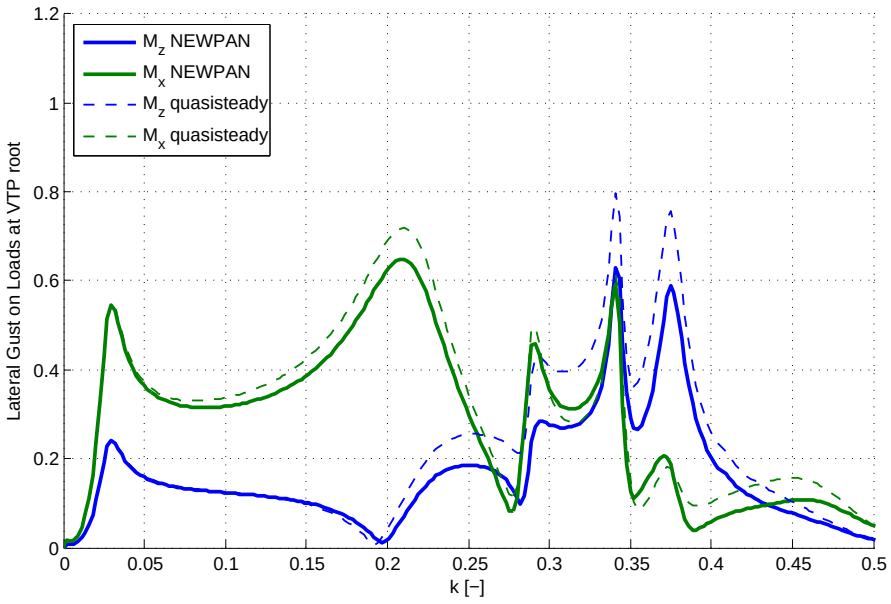

Figure 11. Transfer function: lateral gust input on VTP root bending and torsion moment for the 3D panel method

Figure 11 shows the transfer function of the lateral gust input to the root bending and torsion moments for the root of the vertical tail. The dashed lines represent a quasisteady approximation, where for the entire frequency range the steady AIC $\mathbf{Q}_{jj}(k = 0)$ has been used. As the good accuracy for low frequencies shows, this warrants the use of a quasisteady approximation for flight mechanical analyses, where unsteady aerodynamic effects are negligible.

The first peak corresponds to the dutch roll flight mechanical mode. It was shown in a previous section that this mode is influenced by the presence of inplane aerodynamic forces. As the dutch roll might be excited during gust and turbulence encounters, the resulting loads are affected as well. Hence, the use of aerodynamic methods incorporating these effects, significantly improve the loads analysis also in the case of evaluation in the frequency domain.

V. Summary and Conclusion

A modelling approach, which captures all the relevant effects for flight dynamics, manoeuvre and gust loads analysis has been presented. This includes unsteady aerodynamics, aircraft structural dynamics and static flexibility, nonlinear aerodynamic dependencies, e.g. on angle of attack and important flight mechanical effects like roll-yaw coupling. The latter are usually neglected in typical models for aeroelastic analyses.

Using the proposed scheme, suitable models in the context of aircraft design synthesis and analysis can be deduced, i.e. when repeated simulations in the entire flight envelope are required or many design evaluations are necessary, as e.g. in Multidisciplinary Design Optimization (MDO), for loads computations, performance analysis or control law design.

The seamless integration of the 3D panel method AIC matrices [4] not only allows for consideration of surface pressures instead of pressure differences between upper and lower side, but also to account for inplane aerodynamic forces, which are important for flight mechanical yaw-roll moment coupling or terms related to induced drag.

The AIC-ROM approach [7, 8] allows to consider nonlinear dependencies of the underlying AIC matrices, such as angle of attack or Mach number, by efficient interpolation of a POD based model order reduction. The main advantage over classical pressure ROMs is that only the main nonlinearities need to be considered in the setup, whereas the linear effects such as flexible deformations or rotation rates can be captured by the virtue of the gradient information inherently present in the AIC matrices.

For time domain simulations with unsteady aerodynamic effects, a "physical" Rational Function Approximation [9] without prior multiplication of the differentiation matrices was proposed. This form of RFA allows a physical distinction between quasi steady, added mass and lag terms. This way unsteady aerodynamic contributions can be accounted for if deemed important or traded for faster simulation speeds if a quasi-steady assumption for low frequency excitation is sufficient.

These enabling features of the model integration process can be used in a modular fashion. The models allow for versatile design analyses, as shown in the demonstrated applications regarding flight mechanical modes, "adverse yaw" for manoeuvering flexible aircraft, and loads analysis including flight control laws, for static and dynamic analyses, in the time and frequency domain.

Applications related to active gust and manoeuvre load alleviation, primary flight control design, and performance improvement through lift redistribution are currently in progress.

References

[1] Albano, E. and Rodden, W., "A Doublet-Lattice Method for Calculating Lift Distributions on Oscillating Surfaces in Subsonic Flows," *AIAA Journal*, Vol. 7, No. 2, 1969, pp. 279–285.

[2] Rodden, W., Giesing, J., and Kalman, T., "New Developments and Applications of the Subsonic Doublet-Lattice Method for Nonplanar Configurations," *AGARD Symposium on unsteady aerodynamics for aeroelastic analyses of interfering surfaces*, No. AGARD-CP-80-71, AGARD, 1971.

[3] Rodden, W., Taylor, P., and Jr., S. M., "Further Refinement of the Subsonic Doublet-Lattice Method," *Journal of Aircraft*, Vol. 9, No. 10, 1998, pp. 693–702.

[4] Fiddes, S. P., Burkett, C. W., and Kier, T. M., "An Advanced Panel Method for Compressible Subsonic Unsteady Flow Past Complex Geometries," *International Forum on Aeroelasticity and Structural Dynamics*, No. IFASD-2015-181, 2015.

[5] Waszak, M. R. and Schmidt, D. K., "On the Flight Dynamics of Aeroelastic Vehicles," *AIAA Atmospheric Flight Mechanics Conference*, No. AIAA 86-2077, AIAA, 1986, pp. 120–133.

[6] M. R. Waszak and D. K. Schmidt, "Flight Dynamics of Aeroelastic Vehicles," *Journal of Aircraft*, Vol. 25, No. 6, 1988, pp. 563–571.

[7] Kier, T. M., Verveld, M. J., and Burkett, C. W., "Integrated Flexible Dynamic Loads Models Based on Aerodynamic Influence Coefficients of a 3D Panel Method," *International Forum on Aeroelasticity and Structural Dynamics*, No. IFASD-2015-179, 2015.

[8] Verveld, M. J. and Kier, T. M., "Reduced Order Model of Corrected Aerodynamic Influenceuence Coeffcients for Aircraft Loads Analysis," *58th AIAA/ASCE/AHS/ASC Structures, Structural Dynamics, and Materials Conference, 9-13 January 2017, Grapevine, TX, USA*, AIAA, 2017.

[9] Kier, T. and Looye, G., "Unifying Manoeuvre and Gust Loads Analysis," *International Forum on Aeroelasticity and Structural Dynamics*, No. IFASD-2009-106, 2009.

[10] Kier, T. M., "Integrated Flexible Dynamic Maneuver Loads Models based on Aerodynamic Influence Coefficients of a 3D Panel Method," *56th AIAA/ASCE/AHS/ASC Structures, Structural Dynamics, and Materials Conference, 5-9 January 2015, Kissimmee, FL, USA*, No. AIAA 2015-0185, AIAA, 2015.

[11] Kier, T. M., "An Integrated Model for Lateral Gust Loads Analysis and Dutch Roll Flight Dynamics using a 3D Panel Method," *International Forum on Aeroelasticity and Structural Dynamics*, No. IFASD-2015-179, 2017.

[12] Hedman, S., "Vortex Lattice Method for Calculation of Quasi Steady State Loadings on Thin Elastic Wings," Tech. Rep. Report 105, Aeronautical Research Institute of Sweden, October 1965.

[13] Rodden, W., Harder, R., and Bellinger, E., "Aeroelastic Addition to NASTRAN," Tech. Rep. NASA CR-3094, NASA, March 1979.

[14] Christopher J. Sequeira, D. J. W. and Peraire, J., "Comparing Aerodynamic Models for Numerical Simulation of Dynamics and Control of Aircraft," *44th AIAA Aerospace Sciences Meeting and Exhibit*, No. AIAA 2006-1254, 2006.

[15] Kier, T., "An Integrated Loads Analysis Model including Unsteady Aerodynamic Effects for Position and Attitude dependent Gust Fields," *International Forum on Aeroelasticity and Structural Dynamics*, No. IFASD-2011-052, 2011.

[16] Kier, T., "An Integrated Loads Analysis Model for Wake Vortex Encounters," *International Forum on Aeroelasticity and Structural Dynamics*, No. IFASD-2013-30C, 2013.

[17] Malone, J. and Ruo, S., "LANN Wing Test Program: Acquisition and Application of Unsteady Transonic Data for Evaluation of Three-Dimensional Computational Methods," Tech. Rep. AFWAL-TR-83-3006, Wright Lab., Wright-Patterson AFB, 1983.

[18] Hofstee, J., Kier, T., Cerulli, C., and Looye, G., "A Variable, Fully Flexible Dynamic Response Tool for Special Investigations (VarLoads)," *International Forum on Aeroelasticity and Structural Dynamics*, 2003.

[19] Guyan, R. J., "Reduction of stiffness and mass matrices," *Journal of Aircraft*, Vol. 3, No. 2, 1965, pp. 380.

[20] R. L. Bisplinghoff, H. Ashley, R. L. Halfman, *Aeroelasticity*, Dover Publications Inc., 1955.

[21] Göthert, B., "Ebene und räumliche Strömung bei hohen Unterschallgeschwindigkeiten: Erweiterung der Prandtl'schen Regel," Tech. Rep. Bericht 127, Lilienthal Gessellschaft, 1940.

[22] Harder, R. and Desmarais, R., "Interpolation Using Surface Splines," *Journal of Aircraft*, Vol. 9, No. 2, 1972, pp. 189–191.

[23] Rodden, W. P. and Johnson, E. H., *MSC.Nastran Aeroelastic Analysis User's Guide*, MSC, 1994.

[24] Roger, K. L., "Airplane Math Modeling Methods for Active Control Design," *AGARD Structures and Materials Panel*, No. AGARD/CP-228, AGARD, April 1977, pp. 4–1 – 4–11.

[25] Edwards, J. W., "Applications of Laplace transform methods to airfoil motion and stability calculations," *20th Structures, Structural Dynamics and Materials Conference*, No. AIAA 1979-772, 1979.

[26] Abel, I., "An analytical technique for predicting the characteristics of a flexible wing equipped with an active flutter-suppression system and comparison with wind-tunnel data," Tech. Rep. NASA TP-1367, NASA LARC, 1979.

[27] Karpel, M., "Design for Active and Passive Flutter Suppression and Gust Alleviation," Tech. Rep. NASA CR-3482, NASA, November 1981.

[28] Zimmermann, R. and Görtz, S., "Improved Extrapolation of Steady Turbulent Aerodynamics using a Non-Linear POD-based Reduced Order Model," *Aeronautical Journal*, Vol. 116, No. 1184, 2012, pp. 1079–1100.

[29] European Aviation Safety Agency, *Certification Specifications for Large Aeroplanes CS-25*, Vol. Subpart C - Structure, EASA, 2010.

[30] Leitner, M., Kier, T., and Müller, R., "Einfluss der Flugregelung auf Lasten bei lateralen Manövern," Tech. Rep. DLR-IB-SR-OP-2017-152, DLR, 2017.